Modification of adipose mesenchymal stem cells-derived small extracellular vesicles with fibrin-targeting peptide CREKA for enhanced bone repair

Qi Wu [a,b], Xiaoling Fu [a,c,*], Xian Li [b], Jing Li [b], Weiju Han [b], Yingjun Wang [b,d,**]

[a] School of Biomedical Sciences and Engineering, South China University of Technology, Guangzhou International Campus, Guangzhou, 511442, PR China
[b] National Engineering Research Center for Tissue Restoration and Reconstruction, South China University of Technology, Guangzhou, 510006, PR China
[c] Key Laboratory of Biomedical Engineering of Guangdong Province, South China University of Technology, Guangzhou, 510006, PR China
[d] Key Laboratory of Biomedical Materials and Engineering of the Ministry of Education, South China University of Technology, Guangzhou, 510006, PR China

ABSTRACT

The process of bone repair is highly regulated by a large number of bioactive factors. Thus, a "cocktail" of bioactive factors supplemented to the defect sites is desirable for bone repair. In this regard, small extracellular vesicles (sEVs) derived from mesenchymal stem cells hold great potential in tissue repair. Nevertheless, the poor homing and retention of sEVs greatly limited their possible clinical application. In the present work, DMPE-PEG-CREKA was inserted into the membrane of sEVs released from adipose-derived mesenchymal stem cells to obtain CREKA functionalized sEVs (CREKA-sEVs), which could target fibrin to accumulate and retain in bone defects. Our results showed that CREKA-sEVs, like sEVs, promoted the osteogenic differentiation of BMSCs, the angiogenic property of HUVECs, and modulated the polarization of macrophages in vitro. Furthermore, due to the improved fibrin-binding and retention capacity of CREKA-sEVs, they enhanced the bone repair substantially in the rat femoral defect model. This study provided a new strategy to improve the therapeutic efficiency of sEVs and showed that CREKA-sEVs had great application value in bone tissue repair.

1. Introduction

Bone repair is a complex, well-orchestrated physiological process regulated by a large number of bioactive factors, such as growth factors, cytokines, and chemokines [1,2]. Strategies that help create a microenvironment rich in bioactive factors are therefore considered effective in promoting the process of bone repair. Adding exogenous growth factors, such as BMPs and VEGF, to the defective sites has been widely used and has shown some benefits. For example, the scaffold loaded with the liposomal formulation of BMP-2 induced osteogenic differentiation of MSCs in vitro and enhanced osteogenesis in vivo [3]. Controlled-Release of BMP-2 and VEGF from hydroxylapatite/PLGA scaffold significantly promoted MC3T3-E1 cells proliferation and osteogenic differentiation [4]. However, the delivery of single or two types of growth factors is far from enough to mimic the repairing microenvironment in bone defects, thus often providing suboptimal outcomes.

Small extracellular vesicles (sEVs), including exosomes and other EVs smaller than 200 nm [5,6], contain condensed packages of biological cargo (e.g., miRNA, mRNA, and proteins) that have originated from the parent cells. They serve as the information carrier for intercellular communication by transferring the cargo to target cells, and therefore regulating various physiological and pathological processes [7]. Importantly, due to the diversity of their cargo, sEVs can deliver a unique cocktail of bioactive factors to the defect sites and therefore have the potential to improve the overall microenvironment at the bone defect sites. Recent studies have demonstrated that sEVs derived from MSCs (MSC-sEVs) can facilitate the repair processes of multiple tissues, such as skin [8], bone [9], heart [10], and liver [11]. As regards bone repair, it has been shown that MSC-sEVs can benefit bone repair via enhancing angiogenesis and osteogenesis at the sites of bone defects [12, 13]. Remarkably, MSC-sEVs exerted similar therapeutic effects to their parent cells in many of the studies [14]. have higher stability and less

immunogenicity, compared to MSCs. Meanwhile, they can avoid potential risks of MSCs, like vascular embolism and genetic material variation [15,16]. Hence, sEVs-based cell-free therapy is a promising strategy for bone repair.

However, unmodified sEVs tend to accumulate in organs of the reticuloendothelial system (RES), such as the liver and spleen, few sEVs can be delivered to target tissue through intravenous injection [17,18]. Local delivery increases the concentration of sEVs at the defect sites, but the sEVs are still cleared soon after the administration due to the high local metabolic activity. The poor retention of sEVs greatly limited their possible clinical application. To address this issue, several groups fabricated engineered sEVs endowing them with tissue targeting ability. For example, Kim et al. fabricated anisamide functionalized exosomes to increase the payload delivery to the lung cancer cells which over-expressed sigma receptor [19]. Fibrin is a natural fibrous network formed by the large precursor protein fibrinogen following virtually all forms of tissue damage, to initiate hemostasis and serve as a temporary extracellular matrix [20]. As a near-universal feature of tissue injury, fibrin is an undoubted ideal target for the delivery of sEVs to the defective bone. Fibrin-specific antibodies were once used for fibrin targeting. But now, a variety of fibrin-binding peptides with less immunogenicity and lower cost, have been identified [21]. Among them, a representative one is a pentapeptide cysteine–arginine–glutamic acid–lysine–alanine (CREKA). CREKA exhibits a high affinity to fibrin–fibronectin complexes [22], thereby is a promising bone defect targeting peptide.

Different strategies have been used to functionalize sEVs [23]. For example, Tian et al. conjugated functional ligand c(RGDyK) peptide onto the exosome surface by click chemistry, utilizing the DBCO-Sulfo-NHS linker which reacted with the amino groups of protein on the exosome surface [24]. However, such bioconjugation may impair sEV functions by altering or obscuring the active sites of the surface proteins. In this regard, hydrophobic insertion can be an alternative. Researchers have applied the hydrophobic insertion method for cells modification. For example, Yan et al. use this method to modify ASCs with DMPE-PEG-PBP, which possesses a strong targeted binding ability to injured vessels. It has been shown that this quick and easy approach has no impact on ASCs activities [25]. When this method is used in sEVs, it is based on the hydrophobic effect between sEV membrane lipids and the introduced lipid conjugates. sEVs can be engineered without affecting their biological functions because the insertion of the conjugates into sEVs membrane does not interfere with proteins on the membrane. Paclitaxel (PTX)-loaded exosomes modified with DSPE-PEG-cRGD by hydrophobic insertion have been demonstrated to maintain the integrity of exosomes and improve the curative effects of PTX in glioblastoma via enhanced targeting [26].

Herein, we constructed a "sEVs-CREKA -fibrin" targeting system to enhance the retention of sEVs in the injured and fibrin-rich bone defective sites. "DMPE-PEG-CREKA" was fabricated firstly and inserted into the membrane of sEVs by hydrophobic insertion to construct CREKA-sEVs. The fibrin targeting ability and the regulatory effects of CREKA-sEVs on bone repair were then evaluated both in vitro and in vivo.

2. Experimental section

2.1. Synthesis and characterization of DMPE-PEG-CREKA

CREKA conjugated with fluorescein FAM was synthesized by ChinaPeptides Company (Shanghai, China). DMPE-PEG-Mal synthesized by Beijing Hwrkchemical Company ($M_W \approx 5$ KDa; Beijing, China) was used in the study.

DMPE-PEG-CREKA was prepared via the reaction between thiol groups and maleimide functional groups. Specifically, DMPE-PEG-Mal and CREKA were dissolved in distilled water. DMPE-PEG-CREKA was prepared by mixing the solution of DMPE-PEG-Mal and CREKA at a concentration ratio of 1:2 for 2 h by magnetic stirring. The obtained DMPE-PEG-CREKA was purified using a dialysis tube (MWCO 1K) for 3 days and was dried by freeze-drying. Afterward, DMPE-PEG-CREKA was dissolved in PBS. To determine the chemical structure, DMPE-PEG-Mal and DMPE-PEG-CREKA were dissolved in D_2O and then detected by ^1H NMR spectroscopy operating at 400 MHz at 25 °C.

2.2. Cell culture

Rat adipose-derived mesenchymal stem cells (rASCs) were harvested from SD rats and expanded in a proliferation medium consisting α-MEM, 10% fetal bovine serum (FBS), and 1% penicillin−streptomycin (PS) (Gibco, USA). Rat ASCs between passages 3 and 8 were used for sEVs collection. After reaching 80% confluence, the cells were washed twice with PBS, then cultured for 48 h in an exosome-free medium which contained 10% exosome-depleted FBS (System Biosciences, USA) instead of FBS. Human umbilical vein endothelial cells (HUVECs) (ScienCell, USA) were cultured in Endothelial Cell Medium (ScienCell, USA) containing 5% FBS, 1% endothelial cell growth supplement, and 1% PS. Human bone marrow mesenchymal stem cells (hBMSCs) (Cyagen, China) were cultured in OriCell®Basal Medium (Cyagen, China) with 10% FBS and 1% PS. RAW264.7 was obtained from the Cell Bank of the Chinese Academy of Sciences and cultured in DMEM (Gibco, USA) with 10% FBS. All the cells were placed in a humidified 37 °C, 5% CO_2 incubator.

2.3. Small EVs isolation and modification

After culturing rASCs in an exosome-free medium for 48 h, sEVs were isolated and purified as previously reported [27]. The supernatant from cultured rASCs was collected, centrifuged at $300 \times g$ for 10 min to remove cells, $2000 \times g$ for 20 min to remove dead cells, $10,000 \times g$ for 30 min to eliminate cell debris at 4 °C. The supernatant was then ultracentrifuged at $100,000 \times g$ for 70 min twice to collect and wash sEVs. Then, sEVs in the pellet were resuspended in PBS and were ready to use.

For sEVs modification, sEVs (200 μg/mL) and DMPE-PEG-CREKA (30 μM) were gently mixed and incubated in PBS buffer at 40 °C for 1 h. Afterward, free DMPE-PEG-CREKA was removed by ultracentrifuging twice at $100,000 \times g$ for 70 min.

2.4. Small EVs characterization

The morphology of the obtained sEVs was determined by SEM, 15 μL sEVs or CREKA-sEVs suspension were dropped on copper grids covered with a carbon support film (Zhongjingkeyi Technology, China). It was air-dried for 1 min at room temperature, and then excess fluid was removed with filter paper. The samples were negatively stained with 2% uranyl acetate for 1 min. After that, the stained samples were baked under the lamp for 10 min. At last, TEM (FEI, USA) was performed at 200 kV to visualize and examine the morphology of sEVs and CREKA-sEVs.

The particle size distribution and the CREKA modification efficiency of sEVs were measured with a Flow NanoAnalyzer model type N30E (NanoFCM Inc., China) and analyzed with FlowJo. The background noise of PBS that served as a buffer was first measured. Then, sEVs were diluted to 1 μg/mL and loaded to set the voltages and thresholds for measurements, as well as to provide references for gating in the forward-scatter (FSC) and side-scatter (SSC) channels. Next, the CREKA modification efficiency of sEVs was assessed by detecting the FAM-conjugated CREKA in 1 μg/mL CREKA-sEVs. Illumination was provided by a standard 488 nm red laser, and the fluorescence was collected through a FITC filter.

To observe the morphology of the obtained sEVs, both sEVs and CREKA-sEVs were labeled with PKH26 (4 μM; λex = 565 nm, λem = 594 nm) following the manufacturer's protocol (Sigma, USA), and observed using a confocal laser scanning microscope (CLSM, Leica, Germany)

with excitation at 488 nm and signal collection from 500 to 700 nm to collect FAM fluorescence signals of CREKA. PBS containing PKH26 dye following the same procedures was set as control.

2.5. Western blot

The protein concentrations of sEVs and CREKA-sEVs were determined using a BCA assay kit (Beyotime, China) according to the manufacturer's instructions. sEVs and CREKA-sEVs were lysed with ice-cold RIPA lysis buffer (Beyotime, China) containing a protease inhibitor cocktail (Sigma, USA). Lysates in equal amounts of proteins were separated by SDS-PAGE (Biorad, USA) and then transferred to PVDF membranes (Pall Corporation, USA). After rinsing with TBS (Signalway Antibody, USA) several times and blocking with 5% non-fat milk (BBI, China), the membranes were incubated with anti-CD9 primary antibody (Abcam, ab92726, USA) and anti-TSG101 primary antibody (Abcam, ab125011, USA) overnight. Followed by thoroughly washing, HRP-conjugated secondary antibodies (Signalway Antibody, L3012, USA) were incubated with membranes in darkness for 1 h. ECL reagent (Tanon, China) was added to the membranes to visualize the immunoreactive protein bands, and the ChemiDoc MP imaging system (BioRad, USA) was used to analyze.

2.6. Flow cytometric analysis

The detection of CD86, an M1 surface marker, on RAW264.7 was performed with an Accuri C6 flow cytometer (BD Biosciences, USA), and analyzed with FlowJo. First, macrophages (RAW264.7 cells) were seeded on 48-well plates at a density of 50,000 cells/mL and cultured in a complete conditioned medium for adherence. Then, macrophages were pre-treated with 5 μg sEVs or CREKA-sEVs in the exosome-free conditioned medium for 24 h, while the same volume of PBS buffer was added in the exosome-free conditioned medium as control. Next, macrophages were polarized by LPS (100 ng/mL, Sigma, USA) and IFNγ (20 ng/mL, Peprotech, USA) stimulation for 24 h. Cells were then collected and incubated with PE-conjugated CD86 antibody (BD Biosciences, USA) at 4 °C for 30 min.

2.7. Cellular uptake

For cellular uptake assay, HUVECs or hBMSCs were seeded onto a confocal dish and cultured for 24 h. Then, the PKH26 labeled sEVs and CREKA-sEVs (20 μg) were added to the medium and cultured for another 24 h. Followed by fixing the cells with 4% paraformaldehyde, the nuclei were stained with DAPI (Beyotime, China), and the cytoskeleton was stained with F-actin (AAT Bioquest, USA). Fluorescence imaging was acquired via CLSM. As for RAW264.7, cells were first stimulated by LPS and IFNγ, and then were stained as mentioned above.

2.8. In vitro clot binding and retention of CREKA-sEVs

As previously described [28], fibrinogen (25 mg/mL, Sigma, USA), thrombin (2.5 U/mL, Sigma, USA), CaCl$_2$ (20 mM, Guangzhou Chemical Reagent Factory, China), were mixed and shaken for 1 min to form fibrin clot in a 96 well plate. After being placed in an incubator for 1 h, 100 μL sEVs or CREKA-sEVs labeled with DiD were added onto the fibrin and incubated at 37 °C for another 1 h. At designated time intervals (3 h, 12 h, 24 h, and 48 h), fibrin was washed with PBS twice, and the fluorescence intensity was detected with a plates reader to investigate the release kinetics of sEVs or CREKA-sEVs on fibrin over time. To visualize the retention of sEVs or CREKA-sEVs on fibrin, near-infrared fluorescence (NIRF) images of the fibrin clots were obtained at 0 h and 24 h by IVIS Spectrum/CT imaging system (PerkinElmer, USA) with 620 nm excitation and 670 nm emission filters.

2.9. Transwell migration assay

A transwell migration assay of hBMSCs was conducted in 24-well plates carrying transwell inserts of 8 μm pore size (Corning, USA) according to the manual. Briefly, hBMSCs were resuspended in 200 μL serum-free DMEM at a density of 1 × 10^5 cells/mL and then seeded onto the upper chamber. Either 6 μg sEVs or CREKA-sEVs in 600 μL DMEM containing 10% FBS were added to the lower chamber. The same volume of PBS buffer was added in DMEM containing 10% FBS as control. After 36 h, cells were fixed with 4% paraformaldehyde. Then, the cells were stained with crystal violet. After removing the cells that stayed in the upper chamber with cotton swabs, the migrated cells could be observed under a microscope. The results were exhibited as a mean number of cells per field ± standard deviation.

2.10. ALP staining and quantification

Human BMSCs were cultured in the conditioned medium containing 10 μg/mL sEVs or CREKA-sEVs for 7 days. The medium was replaced every two days. Cells were fixed with 4% paraformaldehyde and stained using an alkaline phosphatase (ALP) staining kit (Beyotime, China). For quantitative analysis of ALP activity, cells were lysed with RIPA buffer and then treated with an ALP kit (Beyotime, China). The OD value was measured at 405 nm. Total cellular protein was measured by the BCA assay to normalize ALP activity. The 405 nm OD value/(total protein amount × incubation time) of each group was calculated.

2.11. Tube formation assay

HUVECs were treated with sEVs or CREKA-sEVs for 48 h. Then, HUVECs were digested and seeded on the matrix gel at a density of 5000 cells/well for 6 h according to the instruction of μ-Slide Angiogenesis (Ibidi, Germany). HUVECs were then dyed with Calcein AM (Yeasen Biotechnology, China) and imaged under a fluorescence microscope.

2.12. RNA isolation and qRT-PCR analysis

Total RNA was extracted from cells with TRIzol reagent (Invitrogen, USA) and quantified with a spectrophotometer (Thermo Scientific, USA). Subsequently, the PrimeScript RT reagent kit (TaKaRa Biotechnology, Japan) was used to perform reverse transcription. Finally, qPCR was conducted on a QuantStudio 6 Flex system (Life Technologies, USA) using the SYBR Green system (Gene Copoeia, USA) to quantify the expression of relative genes. The relative quantification of target genes was normalized to that of GAPDH, and the $2^{-\Delta\Delta Ct}$ method was used to calculate the fold changes. The primers used in the present study were synthesized by TaKaRa and their sequences are listed in Tables S1–S3.

2.13. Surgical procedures

24 female SD rats, aged 6–8 weeks, were used in the study. After anesthesia with sodium pentobarbital (60 mg/kg), the rats had their skin cut longitudinally with a scalpel to expose the lateral position of the distal femur. A circular defect with a diameter of 2.8 mm and a depth of 3 mm was created in the epiphysis at the medial malleolus of the distal femur in the right leg. After flushing the debris, the defects, where the blood clots could be seen, were treated with 40 μL of sEVs, CREKA-sEVs, and PBS, respectively. The sEVs and CREKA-sEVs used in the animal experiment were labeled with DiD (λex = 644 nm, λem = 665 nm, Invitrogen, USA).

2.14. Biodistribution of sEVs In vivo

Two weeks after surgery, NIRF images of the femurs were recorded and analyzed by the IVIS Spectrum system (PerkinElmer, USA) under 620 nm excitation and 670 nm emission filters to detect the
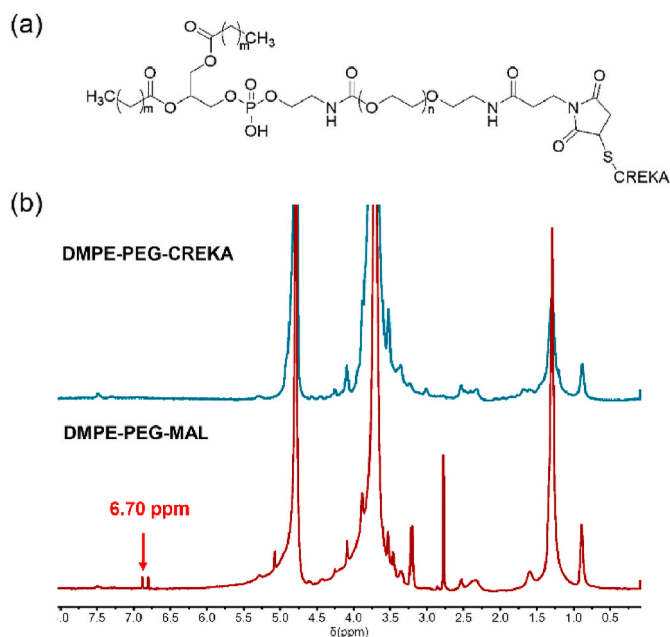
biodistribution of sEVs and CREKA-sEVs.

2.15. Micro-CT and histological assessment

Four weeks after surgery, rats were sacrificed and their right femurs were harvested for Micro-CT analysis. After washing with PBS, the samples were fixed in 4% paraformaldehyde for 24 h and then analyzed by Micro-CT (ZKKS-MCT-Sharp, China). A voxel resolution of 20 μm and a 70 kV and 100 μA beam with a 100 ms integration time were used for scanning. 3D model of the femurs and quantitative analysis was performed by Micro-CT Reconstruction software.

For histological assessment, HE staining and Masson staining were performed to evaluate the new bone volume and structure of bones 4 weeks post-surgery. To determine the expression of OCN and CD31, immunohistochemical staining was also performed 4 weeks post-surgery. As immune response occurs generally early in bone repair, CD86, CD206, iNOS and ARG-1 were assessed by immunohistochemical staining 2 weeks post-surgery. The quantification of OCN, CD31, CD86, CD206, iNOS and ARG-1 was performed by ImageJ. Briefly, images of randomly selected fields of view at 200x magnification were imported into ImageJ and analyzed using IHC Toolbox plugin. The area of yellow-brown signal versus the view area was determined to quantify expression.

2.16. Statistical analysis

Independent experiments with at least triplicates per group were

Fig. 1. Characterization of DMPE-PEG-CREKA. (a) Chemical structure of DMPE-PEG-CREKA, m = 12; (b) ^{1}H NMR spectrum of DMPE-PEG-Mal and DMPE-PEG-CREKA. The arrow indicated free maleimide.
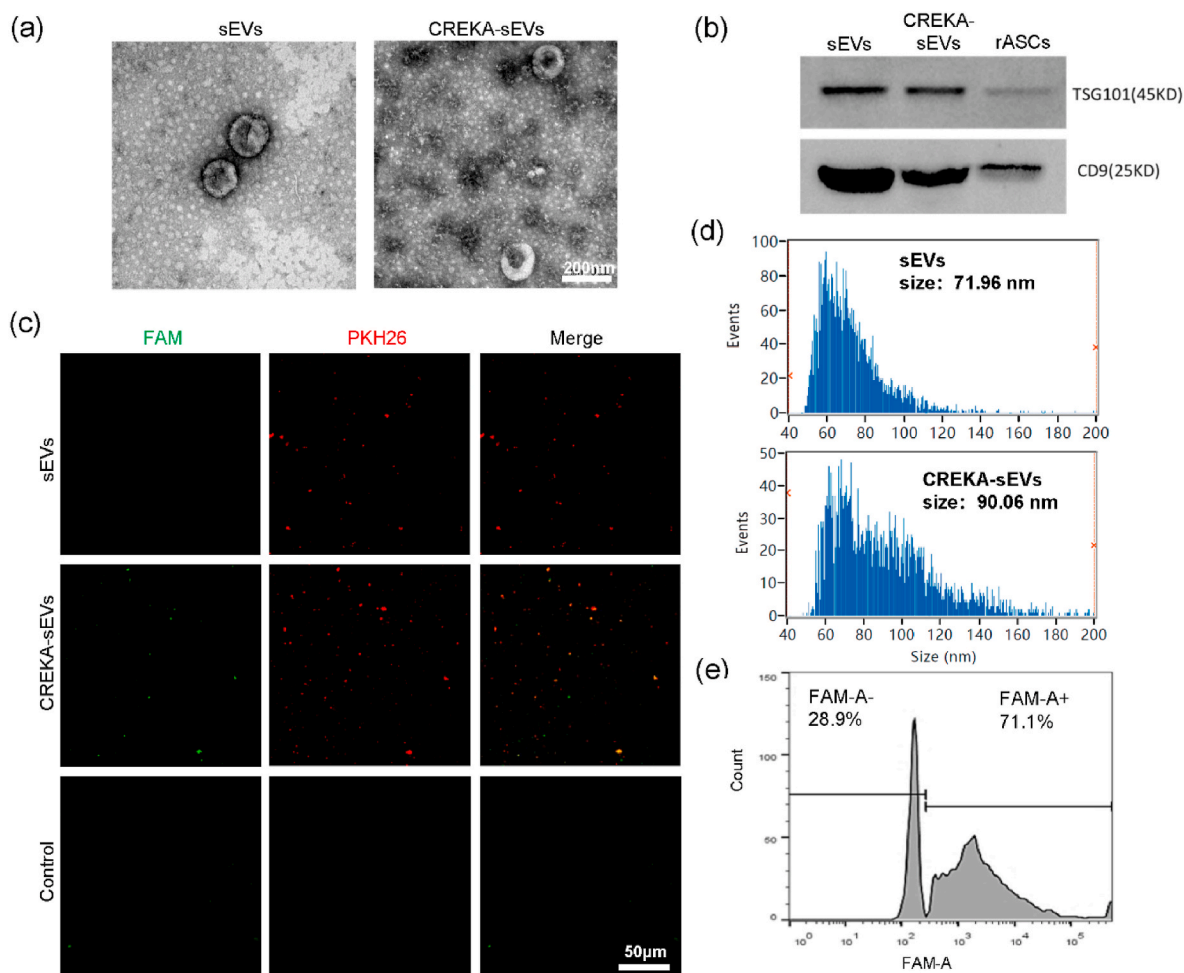

Fig. 2. Characterization of sEVs and CREKA-sEVs. (a) TEM images. Scale bar: 200 nm; (b) WB analysis of TSG101 and CD9; (c) CLSM images. Red: PKH26 labeled sEVs. Green: FAM labeled CREKA. Scale bar: 50 μm; (d) Particle size distribution of sEVs and CREKA-sEVs; (e) CREKA modification efficiency of sEVs.
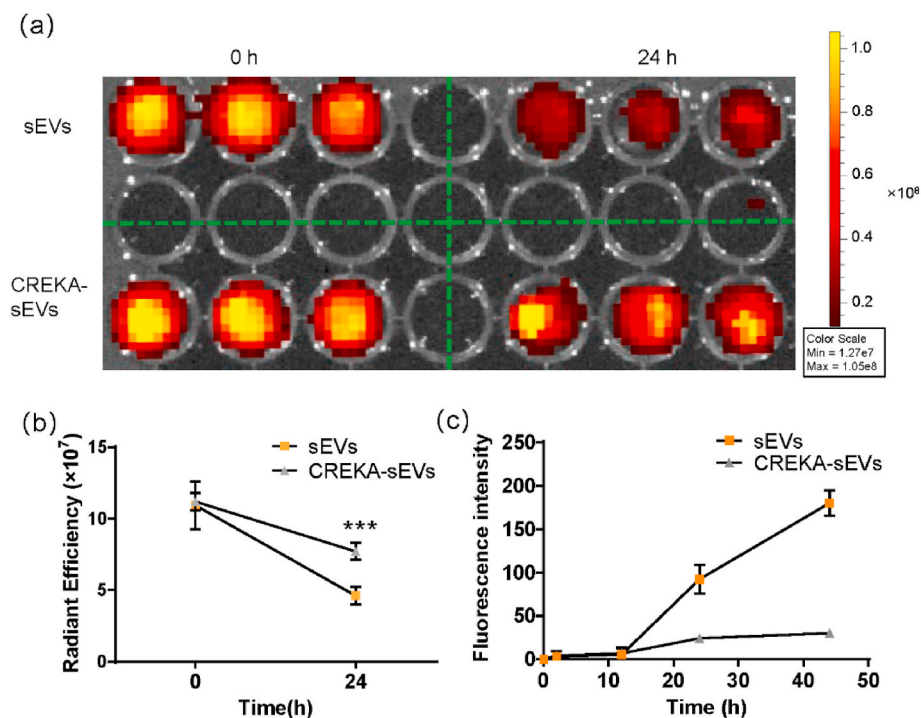
Fig. 3. In vitro fibrin binding and retention of sEVs and CREKA-sEVs. (a) DiD-labeled sEVs and CREKA-sEVs bound onto the fibrin determined by NIRF; (b) Semi-quantitative analysis of the amount of sEVs and CREKA-sEVs bound onto the fibrin; (*Statistically significant, ***$p < 0.001$ vs sEVs) (c) Release kinetics of sEVs and CREKA-sEVs from the fibrin determined by a plate reader.

performed three times to assure repeatability ($n \geq 3$). All values were expressed as the mean $\pm$ standard deviation (SD) and analyzed using Prism 6 software (GraphPad). Statistical significance between two groups was determined using an independent unpaired two-tailed Student's t-test. Comparisons among more than two groups were analyzed using one-way AVONA. For multiple comparisons, Turkey's correction was applied. When multiple results were compared against the control group, Dunnett's correction was applied. P values of <0.05 were considered statistically significant.

3. Results

3.1. Characterization of CREKA-sEVs

In our work, CREKA was conjugated to DMPE-PEG-Mal through the reaction between the thiol group of CREKA and the Mal group. The chemical structure and ^{1}H NMR spectrum of the resulting DMPE-PEG-CREKA were shown in Fig. 1. D_2O signals at 4.65 ppm acted as a reference to determine chemical shifts. The disappearance of the peak at 6.70 ppm for the maleimide protons indicated the successful conjugation of CREKA to DMPE-PEG-Mal.

To obtain CREKA-sEVs, sEVs were isolated from the culture medium of rASCs and then incubated with DMPE-PEG-CREKA. TEM analysis revealed that both sEVs and CREKA-sEVs were double-layer vesicles with intact membrane structure and typical cup shape (Fig. 2a). WB analysis confirmed the expression of sEVs surface markers CD9 and cytosolic protein TSG101 in both sEVs and CREKA-sEVs. The levels of both CD9 and TSG101 were comparable in sEVs and CREKA-sEVs, while significantly lower in rASCs (Fig. 2b), indicating a high abundance of exosomal marker proteins in sEVs and CREKA-sEVs. To visualize the modification, sEVs and CREKA-sEVs both labeled with PKH26 were observed under CLSM (Fig. 2c). Obvious red signals were detected in the sEVs and the CREKA-sEVs group. On the contrary, no red signal was observed in the control group (PBS containing PKH26 following the same procedure of centrifugation was set as the control group),

excluding the possibility that the observed red signals came from the fluorescent dye itself. In the CREKA-sEVs group, the fluorescence signals of FAM-labeled CREKA and PKH26 labeled sEVs co-located to a large extent, further confirming the successful modification of DMPE-PEG-CREKA on sEVs. The particle concentration, particle size distribution of sEVs and CREKA-sEVs together with the modification efficiency were determined through nanoflow cytometry (NanoFCM). The results showed that the particle-to-protein ratio of sEVs was 3.89×10^9 particles/µg and that of CREKA-sEVs was 5.00×10^9 particles/µg. As shown in Fig. 2d, the average diameter of sEVs was 71.96 nm, and that of CREKA-sEVs was 90.06 nm, which was relatively larger. The particle size distribution of both groups was still in the range of 50–200 nm and met the definition of sEVs. Unlike the sEVs group, it could also be observed that there were two main peaks in the particle size distribution of the CREKA-sEVs group, indicating the heterogeneity of the particles in the CREKA-sEVs group. Similarly, the fluorescence histogram of CREKA-sEVs also showed two peaks with 71.1% particles being FAM positive, Therefore, the CREKA modification efficiency was 71.1%. The above results illustrated that sEVs derived from rASCs were successfully isolated, and modified with CREKA.

3.2. In vitro clot binding and retention of CREKA-sEVs

The binding and retention capacity of CREKA-sEVs on fibrin were evaluated. As shown in Fig. 3a, both sEVs and CREKA-sEVs groups exhibited strong red fluorescence signals, demonstrating that sEVs and CREKA-sEVs could bind onto the fibrin clot. However, the fluorescence intensity greatly decreased in the sEVs group after 24 h, while in the CREKA-sEVs group, the signals were still strong, although decreased a little compared to that at 0 h. The semi-quantitative analysis confirmed that the fluorescence intensity of CREKA-sEVs was about 1.7 times that of sEVs at 24 h (Fig. 3b).

We next analyzed the release kinetics of sEVs and CREKA-sEVs from fibrin by measuring the fluorescence intensity of the supernatant. We found that the amount of sEVs and CREKA-sEVs shedding from the fibrin
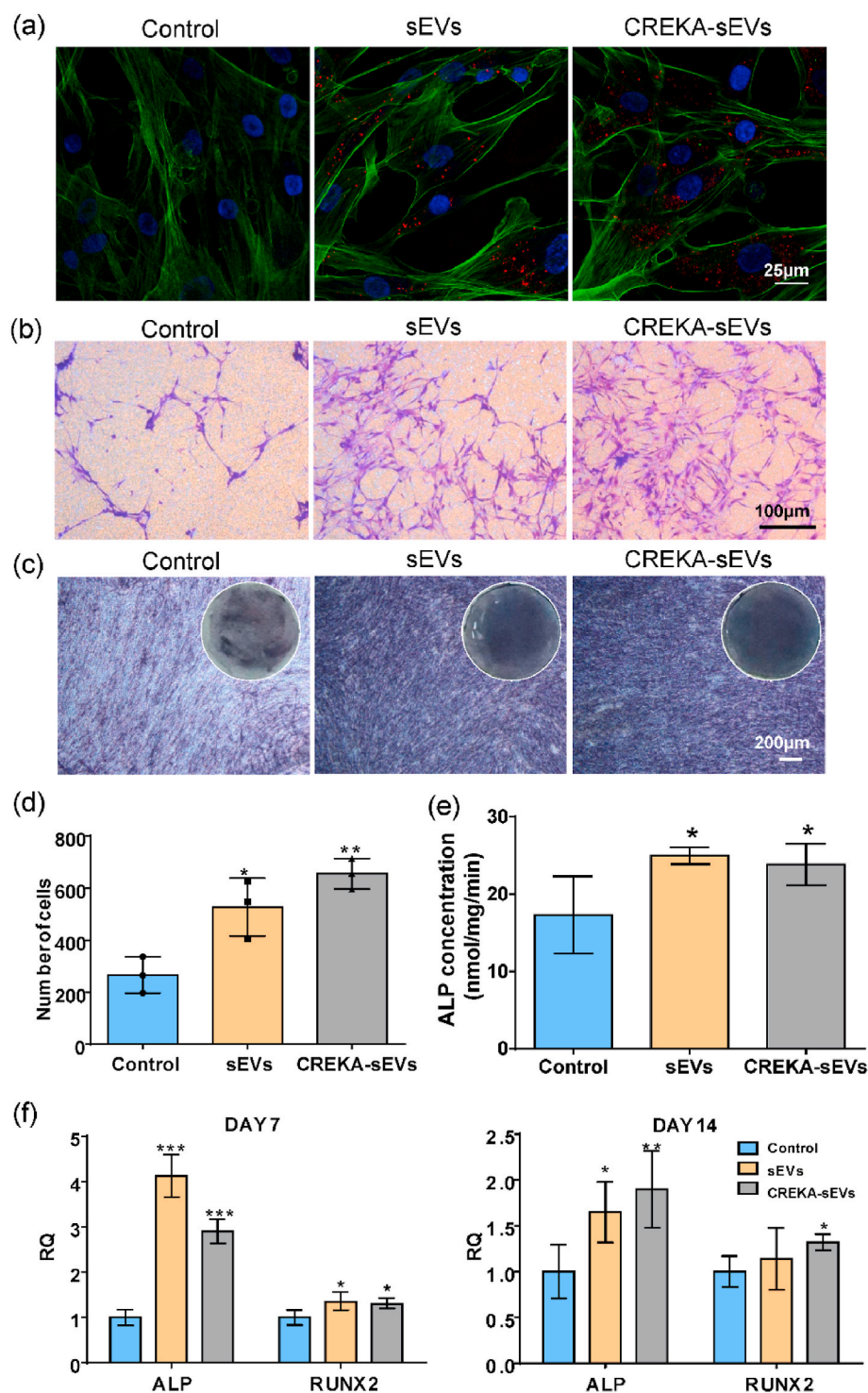
Fig. 4. Regulation of CREKA-sEVs on hBMSCs in vitro. (a) Internalization of sEVs and CREKA-sEVs by hBMSCs. Red: PKH26 labeled sEVs and CREKA-sEVs. Green: F-actin. Blue: Nuclei. Scale bar: 25 μm; (b) Representative pictures of hBMSCs migration stimulated by10 μg/mL sEVs and CREKA-sEVs; (c) Representative images of ALP staining of hBMSCs on day 7; (d) Semi-quantitative analysis of hBMSCs migration; (e) ALP activity of hBMSCs on day 7; (f) Key osteogenic genes expression of hBMSCs on day 7 and 14 (ALP, RUNX2). (*Statistically significant, *$0.01 < p < 0.05$, **$0.001 < p < 0.01$, ***$p < 0.001$ vs Control).

surface was very small within the first 12 h. As time went on, the fluorescence intensity of the sEVs group significantly increased, indicating that many sEVs were released from the fibrin. On the contrary, the fluorescence intensity of the CREKA-sEVs group stayed relatively low during the whole experimental period (48 h). The fluorescence intensity of the CREKA-sEVs group was about 4 times lower than that of the sEVs group at 48 h. Apparently, the majority of CREKA-sEVs were retained on the fibrin for at least 48 h. These results showed that CREKA modification enhanced the retention capacity of sEVs.

3.3. Biological effects of CREKA-sEVs on BMSCs In vitro

BMSCs are the key player during the whole process of bone repair. Thus, we firstly investigated the biological effects of CREKA-sEVs on hBMSCs. In general, sEVs regulate cell-to-cell communication via endocytosis. As shown in Fig. 4a, both sEVs and CREKA-sEVs could be internalized by hBMSCs, and they were mostly distributed in the cytoplasm.

Next, the migration of hBMSCs was determined by the transwell assay. As Fig. 4b and c showed, treatment of 10 μg/mL sEVs or CREKA-sEVs increased the number of cells that migrated to the lower surface of
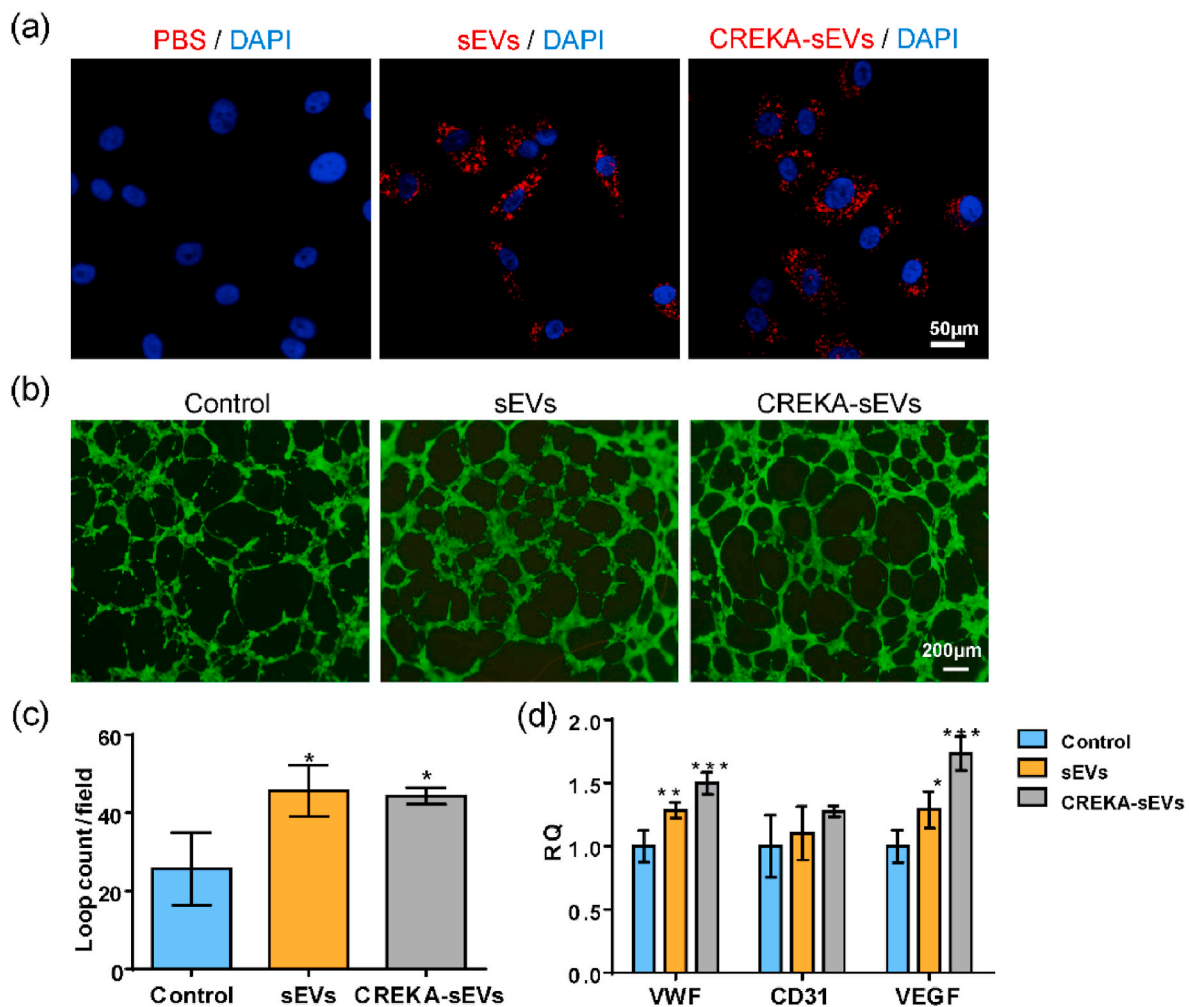
Fig. 5. Regulation of HUVECs by CREKA-sEVs in vitro. (a) Cellular internalization of CREKA-sEVs by HUVECs. Red: PKH26 labeled sEVs and CREKA-sEVs. Blue: Nuclei. Scale bar: 50 μm; (b) In vitro tube formation of HUVECs. Scale bar: 100 μm; (c) Quantification of loop counts; (d) Key angiogenic gene expression of HUVECs. (*Statistically significant, *0.01 < p < 0.05, **0.001 < p < 0.01, ***p < 0.001 vs Control).

the transwells. But there was no significant difference between the sEVs and CREKA-sEVs groups. The result indicated that CREKA modification had no impact on the improvement of hBMSCs migration by sEVs. In addition, the number of migrated cells was almost the same with and without 5 μg/mL sEVs, while 10 μg/mL sEVs significantly increased cell migration, and 15 μg/mL sEVs stimulated cell migration even greater (Fig. S1). Clearly, the promotion of hBMSCs migration was positively correlated with sEVs concentration in the range of 5–15 μg/mL.

Next, the effects of sEVs on the osteogenesis of hBMSCs were investigated. After 7 days of culture, ALP activity was measured. As shown in Fig. 4d, the ALP activities in the sEVs and CREKA-sEVs groups were significantly higher than that in the control group. Quantitative results were in line with the staining results, suggesting that sEVs and CREKA-sEVs promoted the ALP activity of hBMSCs. Consistently, the mRNA expression of ALP and RUNX2 was also upregulated in the sEVs and CREKA-sEVs groups on day 7. On day 14, the stimulatory expression of ALP by sEVs and CREKA-sEVs was still observed, although weaker than that on day 7. Meanwhile, only RUNX2 in the CREKA-sEVs group kept at the elevated level compared to the other two groups on day 14. Collectively, these results revealed that both sEVs and CREKA-sEVs could induce osteogenic differentiation of hBMSCs.

3.4. Biological effects of CREKA-sEVs on HUVECs In vitro

Angiogenesis is an important biological process that can affect the

outcomes of bone regeneration because newly formed vessels are necessary for oxygen and nutrition supply to defect sites [29].

To establish a biological basis for the potential functional influence of CREKA-sEVs on HUVECs, the internalization was observed by CLSM. Similar to hBMSCs, Fluorescence images revealed that HUVECs could internalize PKH26 labeled CREKA-sEVs (Fig. 5a). To assess the regulatory effects of sEVs and CREKA-sEVs on the angiogenic ability of HUVECs, the tube formation of HUVECs was evaluated. As shown in Fig. 5b, HUVECs treated with sEVs formed more complete tubular structures compared to that of the control, and this effect on HUVECs was not impaired by CREKA modification. The expression of key angiogenic genes, including vWF and VEGF, was significantly increased in HUVECs treated with either sEVs or CREKA-sEVs. These results suggested that sEVs and CREKA-sEVs could promote the differentiation and angiogenic properties of HUVECs.

3.5. Effects of CREKA-sEVs on macrophage polarization

Immunomodulation is another important process during bone repair, so the internalization and phenotype switch of macrophages were investigated. It was confirmed that like hBMSCs and HUVECs, RAW264.7 could also internalize sEVs and CREKA-sEVs (Fig. S2). We first explored the regulatory effects of sEVs and CREKA-sEVs on M1 macrophages. As shown in Fig. 6a and b, macrophages post-treated with either sEVs or CREKA-sEVs expressed higher levels of anti-inflammatory
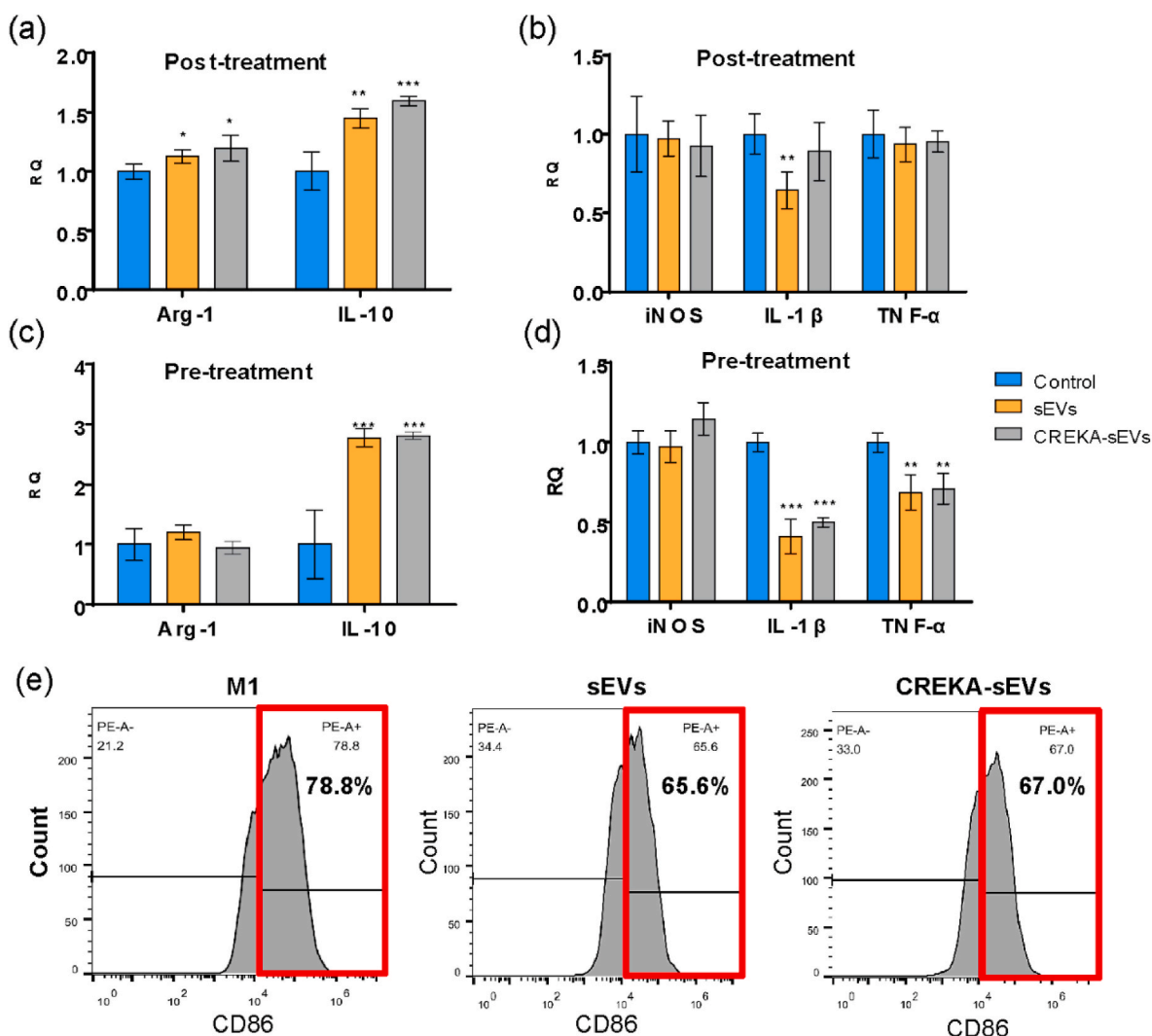
Fig. 6. Regulation of CREKA-sEVs on the M1 polarization of macrophages. (a–b) Expression of key inflammation related genes by M1 macrophages post-treated with sEVs or CREKA-sEVs; (c–d) Expression of key inflammation related genes by M1 macrophages pre-treated with sEVs or CREKA-sEVs; (*Statistically significant, *$0.01 < p < 0.05$, **$0.001 < p < 0.01$, ***$p < 0.001$ vs Control) (e) FCM analysis of M1 macrophages pre-treated with sEVs or CREKA-sEVs.
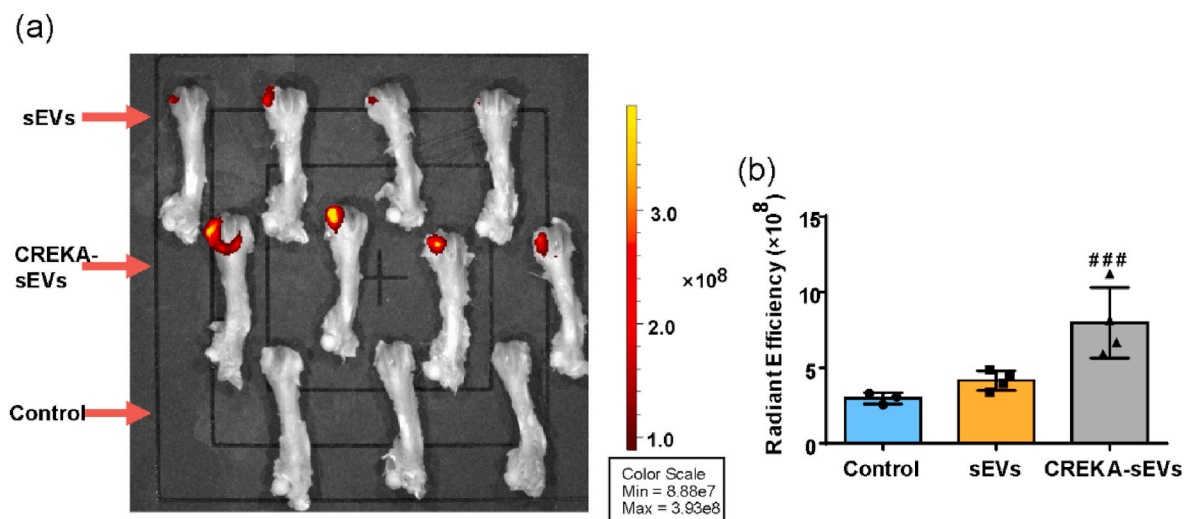

Fig. 7. Retention of CREKA-sEVs in vivo. (a) NIRF image; (b) Quantitative analysis. (#Statistically significant, ###$0.001 < p < 0.01$ vs sEVs).
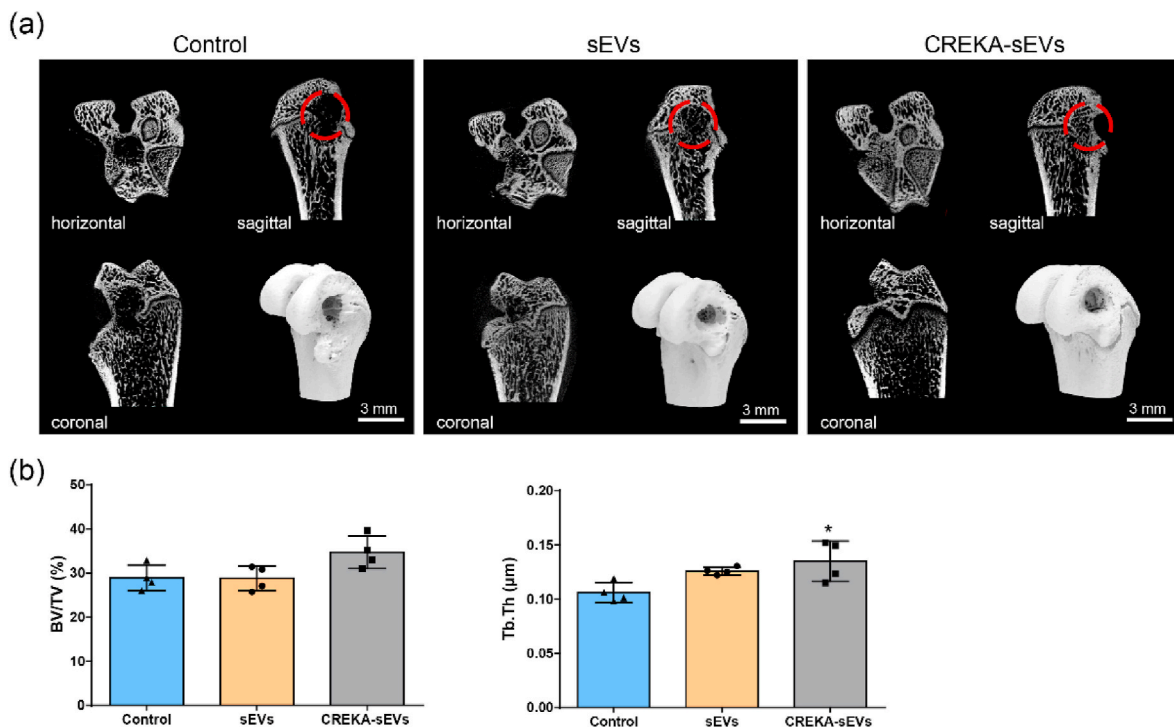
Fig. 8. Micro-CT analysis of the femurs 4 weeks after surgery. (a) Three-dimensional reconstruction and CT images of the bone defects with different treatments (coronal plane, sagittal plane, and horizontal plane); (b) Quantitative analysis by micro-CT. (*Statistically significant, *0.01 < p < 0.05 vs Control).

factors including Arg-1 and IL-10, while sEVs inhibited the expression of inflammatory factor IL-1β, compared to the control. We then explored if the pre-incubation of M0 macrophage with sEVs and CREKA-sEVs could affect their functions. According to Fig. 6c, the pre-treatment of either sEVs and CREKA-sEVs promoted the expression of IL-10 and decreased the expression of IL-1β and TNF-α. Flow cytometry analysis (FCM) was performed to further confirm the effects of sEVs and CREKA-sEVs pre-treatment on macrophage polarization (Fig. 6e). Compared with the control (M1 macrophages without any pre-treatment), the group in which macrophages pre-incubated with either sEVs or CREKA-sEVs had fewer CD86 positive cells. Our results demonstrated that sEVs and CREKA-sEVs both suppressed M1 polarization of macrophages. The effects of sEVs and CREKA-sEVs are comparable without significant difference.

3.6. Retention of CREKA-sEVs in bone defect sites

In order to investigate whether CREKA modification could enhance the retention rate of sEVs in vivo, we labeled sEVs and CREKA-sEVs with DiD and tracked their biodistribution in a femoral defect model two weeks after surgery. As shown in Fig. 7a, the defect was located at the medial malleolus of the distal femur, at the upper left corner of each femur. Obviously, the sEVs group showed weak fluorescence, while the CREKA-sEVs group had more intensive fluorescence. Quantitative analysis showed fluorescence intensity of the CREKA-sEVs group was about 1.9 times that of the sEVs group, indicating that more CREKA-sEVs were retained in the defect for at least two weeks.

3.7. Regulation of bone repair by CREKA-sEVs

The femur samples were scanned by micro-CT 4 weeks after surgery. As Fig. 8a showed, the size of the bone defect in the control group was nearly the same as the original one (shown in the red circle). Meanwhile, the trabecular structure could be found loosely appearing in the defect of the sEVs group. In the CREKA-sEVs group, there were new bones with dense trabecular structure in defect and the size of the defect decreased

significantly. As for bone volume fraction (BV/TV), CREKA-sEVs treatment slightly increased the value of BV/TV, compared to the sEVs and the control group. CREKA-sEVs treatment also increased the value of trabecular thickness, compared to the control group.

The bones were also harvested and observed via HE staining and Masson staining 4 weeks after surgery (Fig. 9). The HE staining results showed that new tissue has filled the defect in both sEVs and CREKA-sEVs groups, while there were still large cavities at the defect site in the control group. Besides, more mature bone tissue with orderly bone trabecular structure and relatively less immature bone tissue could be observed in the CREKA-sEVs group, compared to the sEVs group. Similarly, the Masson staining further confirmed the above results (Fig. 9b).

CD31 is a surface marker for endothelial cells. As shown in Fig. 10a, there was little CD31 expression at the site of cavities in the control group. A few yellow-brown circles which indicated blood vessels could be observed in immature bone tissue as pointed by the orange arrows in the sEVs group. Significantly more blood vessels were detected in the CREKA-sEVs group. The quantitative results showed that the CREKA-sEVs induced more CD31 expression than the sEVs and control groups (Fig. 10b). This result indicated that CREKA-sEVs improved angiogenesis but sEVs did not. Besides, the expression of key osteogenic marker OCN was evaluated. Compared to the control, a higher expression level of OCN was observed in the bone tissue treated with either CREKA-sEVs or sEVs, especially in the immature bone tissue area (Fig. 10a and b).

To investigate the inflammatory response during bone repair, immunohistochemical staining of CD86, CD206, ARG-1, and iNOS was performed 2 weeks after surgery. As shown in Fig. 11a, ARG-1 was mostly distributed in the immature bone tissue in the sEVs and the CREKA-sEVs group. However, only the CREKA-sEVs group exhibited a significantly larger ARG-1 area fraction than the control group as quantitative analysis suggested (Fig. 11b). As for iNOS expression, positive staining was weak in all groups and the quantitative result showed no significant difference among groups. Thus, CREKA-sEVs treatment increased the expression of the anti-inflammatory and pro-repair factor ARG-1 in the bone tissue, which may help resolve the
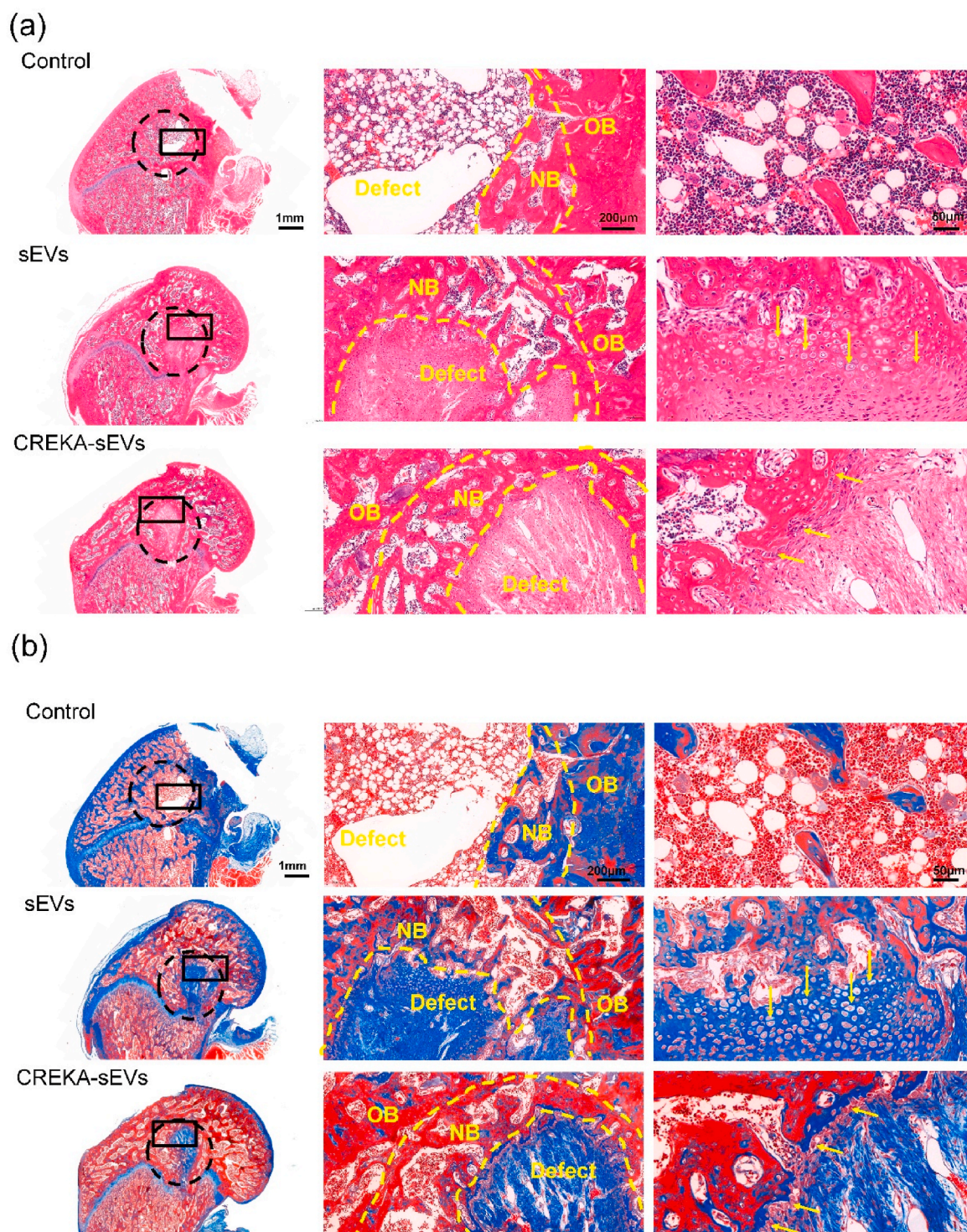
Fig. 9. Representative images of histological staining of the bone tissue. (a) HE staining; (b) Masson staining. NB: New bone. OB: original bone. The black dotted circle in the left column (15x magnification) indicates the area of drilling trauma during surgery. Images in the second column represented the enlarged area (100 x magnification) of the black rectangle in the left column. Images in the right column represented the enlarged area (300 x magnification) of the junction between the new bone and the defect area. Yellow dotted lines were used to indicate the boundary between defect, new bone, and original bone. Yellow arrows pointed to chondrocytes.

inflammatory responses and enhance the repair process. CD206 staining results indicated tissues of CREKA-sEVs had more M2 macrophages in defect (Fig. S3).

4. Discussion

Different strategies have been developed to treat tissue damage and achieved some inspiring outcomes [30,31]. In the past decade, sEVs derived from MSCs have emerged as a promising candidate for tissue repair, and have been proved to exhibit effective therapeutic effects in
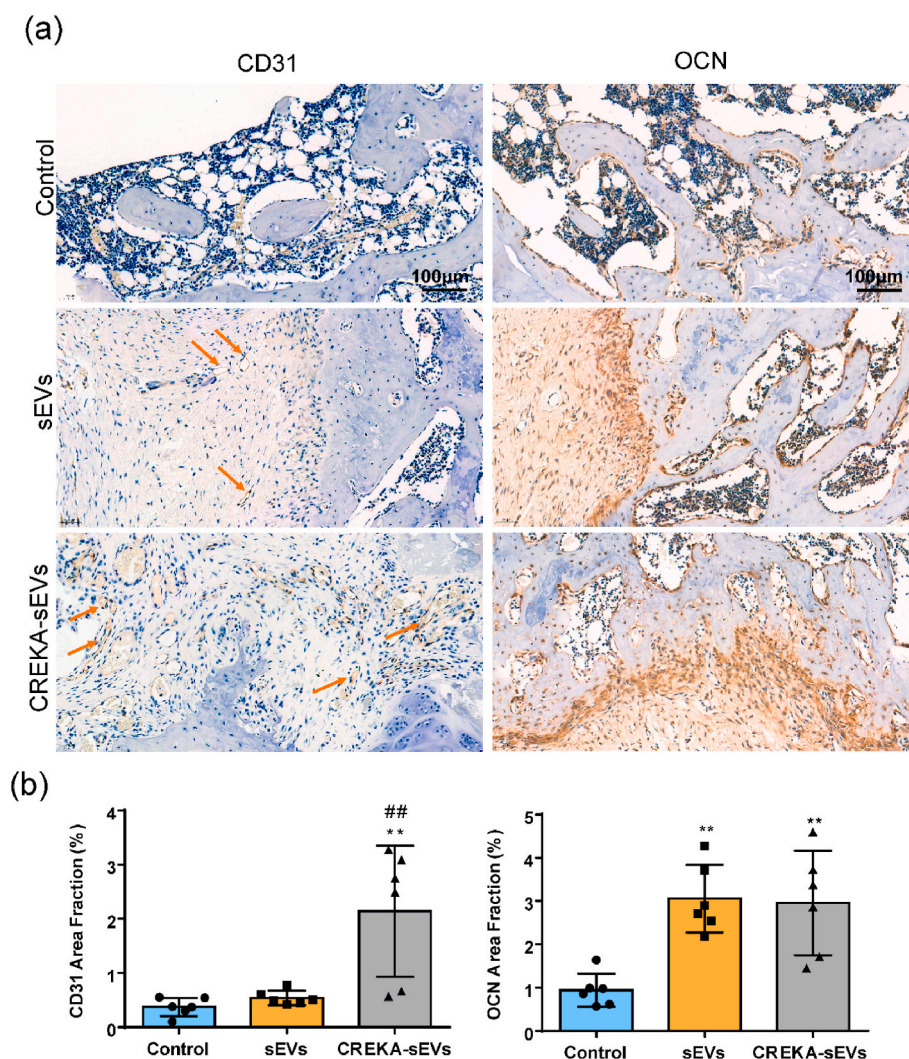
Fig. 10. Immunohistochemical staining of CD31 and OCN in the bone tissue 4 weeks after surgery. (a) Representative images of CD31 and OCN staining. (b) Quantitative analysis of the CD31 and OCN positive area. (*Statistically significant, **$0.001 < p < 0.01$ vs Control; ##$0.001 < p < 0.01$ vs sEVs).

many studies. However, their application is severely limited due to their poor homing and retention capacity to the defect sites. In this study, we fabricated CREKA functionalized rASCs-derived sEVs to endow sEVs with the capacity of fibrin targeting and binding for the treatment of bone defects. By using the hydrophobic insertion method for the modification, DMPE-PEG-CREKA was successfully inserted into the membrane of sEVs without shielding or affecting the functions of proteins on sEV surface (Figs. 1 and 2). As expected, CREKA-sEVs exhibited a stronger fibrin binding ability and slower release profile, compared to the unmodified sEVs (Figs. 3 and 7). Although, the retention of CREKA-sEVs in vivo was currently only evaluated in the rat bone defect model, the CREKA-sEVs-fibrin targeting system was supposed to be effective for other tissue damages, considering that the formation of fibrin clots was a near-universal feature of tissue injury.

To investigating the therapeutical effects of CREKA-sEVs on bone repair, their regulatory effects on the key players in the repairing process, including BMSCs, endothelial cells (HUVECs), and macrophages (RAW264.7), were evaluated systematically. Our in vitro data showed that the bioactivities of sEVs were well preserved and even enhanced after CREKA modification. Specifically, CREKA-sEVs exhibited comparable chemotactic and osteogenic effects with sEVs in vitro, evidenced by the promoted hBMSCs migration, ALP activity, and osteogenic gene expression (ALP and RUNX2) (Fig. 4). The underlying mechanism of sEVs-induced osteogenic effect involved the regulation of osteogenic

related signaling pathways, PI3K/Akt for example, in recipient cells [32]. The observed osteogenic effects of sEVs might be mainly attributed to their cargos. A variety of miRNAs, cytokines, growth factors, and other substances contained in sEVs might be involved in the regulation of osteogenic related signaling pathways in hBMSCs, thus influencing the expression of osteogenic related genes including RUNX2 and ALP. Our rASC- sEVs contained a variety of micro RNAs, including osteogenic miRNAs like miR-130a-3p [33] as shown in our previous study [34].

As another crucial event during bone repair, angiogenesis was also regulated by sEVs. Our results showed that both sEVs and CREKA-sEVs stimulated HUVECs to express the angiogenic genes (vWF and VEGF) and form more vascular-like loop structures in vitro (Fig. 5). The improvement of angiogenesis by rASC-sEVs had been confirmed by several studies [35,36]. Micro RNA 126a-5p and other angiogenic related miRNAs enriched in sEVs may contribute to the angiogenic effects of sEVs [34].

In addition to the osteogenic differentiation of MSCs and new blood formation, the inflammatory response plays an important role in determining the repair outcome. Thus, the phenotypic change of macrophages (RAW264.7) was assessed, because macrophages are the main immune cells in the defect sites. Consistent to many other studies [37–39], our results showed that sEVs secreted by ASCs significantly increased the expression of IL-10 in macrophages (Fig. 6), which was expressed at high level by M2 macrophages and participated in the
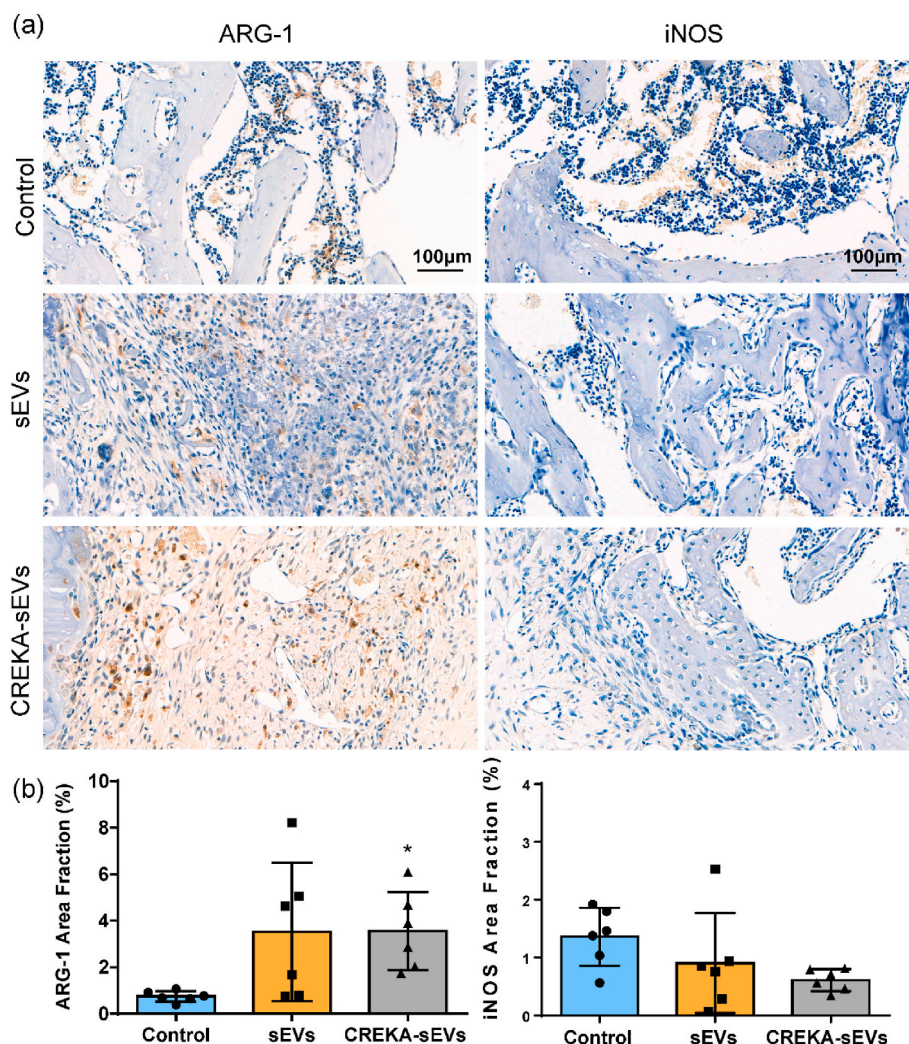
Fig. 11. Immunohistochemical staining of ARG-1 and iNOS in the bone tissue 2 weeks after surgery. (a) Representative images of ARG-1 and iNOS staining. (b) Quantitative analysis of ARG-1 and iNOS positive area. (*Statistically significant, *$0.01 < p < 0.05$ vs Control).

inhibition of inflammation [40]. Surprisingly, the expression of iNOS did not change after sEVs treatment. One possible explanation was that sEVs triggered macrophages to polarize towards M2b phenotype. One typical feature of M2b macrophages, a subtype of M2, is the high expression of IL-10, iNOS, IL-6, etc [41]. The active signal transducer and activator of transcription 3 (STAT-3) enclosed in ASC-sEVs have been demonstrated to be involved in driving the M2 polarization of macrophages through the transactivation of ARG-1 [38].

While sEVs and CREKA-sEVs exhibited similar regulatory effects on cells related to bone repair in vitro, the repair outcome in the rat femoral condyle defect model was significantly improved by CREKA-sEVs, compared to sEVs (Figs. 8 and 9). Although sEVs increased the expression of OCN, they provided limited benefit to bone repair. Instead, the in-situ injection of CREKA-sEVs accelerated bone regeneration in many ways, including stimulating angiogenesis and osteogenesis, as well as modulating the inflammatory responses. This difference between the sEVs and CREAK-sEVs group could be explained by the higher binding capacity and retention of CREKA-sEVs in the defect compared with sEVs. Small EVs have been reported to promote tube formation and the expression of angiogenic-related factors in endothelial cells in a dose-dependent manner [42,43]. The in vivo results further confirmed CREKA modification was an effective and simple way to enhance the therapeutic effectiveness and efficiency of sEVs.

5. Conclusion

In this study, CREKA-sEVs were fabricated by inserting DMPE-PEG-CREKA into the sEVs membrane via the hydrophobic insertion method. The obtained CREKA-sEVs were able to target and bind to fibrin effectively while preserving the bioactivities of sEVs. Although CREKA-sEVs showed comparable regulatory effects with sEVs on BMSCs, HUVECs, and RAW264.7, they remarkably enhanced the bone repair in the rat femoral defect model.

Ethics approval and consent to participate

The study was approved by the Ethics Committee (Institutional Animal Care and Use Committee of Ruige Biotechnology, China) Ethical approved number is IACUC 20220123-01.

Associated content

Primers used in qPCR assays; transwell assay of hBMSCs treated with different concentrations of sEVs; images of RAW264.7 internalizing sEVs or CREKA-sEVs; images of CD86 and CD206 staining.

CRediT authorship contribution statement

Qi Wu: Writing – original draft, Preparation, Methodology,

Investigation, Visualization. **Xiaoling Fu:** Writing – review & editing, Validation, Conceptualization. **Xian Li:** Investigation. **Jing Li:** Resources. **Weiju Han:** Investigation. **Yingjun Wang:** Supervision, Funding acquisition.

Declaration of competing interest

There are no conflicts to declare.

Acknowledgments

Appendix A. Supplementary data

Supplementary data to this article can be found online at https://doi.org/10.1016/j.bioactmat.2022.05.031.

References

[1] L. Polocorrales, M. Latorreesteves, J.E. Ramirezvick, Scaffold design for bone regeneration, J. Nanosci. Nanotechnol. 14 (2014) 15–56.

[2] A.A. El-Rashidy, J.A. Roether, L. Harhaus, et al., Regenerating bone with bioactive glass scaffolds: a review of in vivo studies in bone defect models, Acta Biomater. 62 (2017) 1–28.

[3] M. Mohammadi, M. Alibolandi, K. Abnous, et al., Fabrication of hybrid scaffold based on hydroxyapatite-biodegradable nanofibers incorporated with liposomal formulation of BMP-2 peptide for bone tissue engineering, Nanomed. UK 14 (2018) 1987–1997.

[4] T. Wang, S. Guo, H. Zhang, Synergistic effects of controlled-released BMP-2 and VEGF from nHAC/PLGAs scaffold on osteogenesis, BioMed Res. Int. 2018 (2018), 3516463.

[5] C. Thery, K.W. Witwer, E. Aikawa, et al., Minimal information for studies of extracellular vesicles 2018 (MISEV2018): a position statement of the International Society for Extracellular Vesicles and update of the MISEV2014 guidelines, J. Extracell. Vesicles 7 (2018), 1535750.

[6] Y.F. Zhang, J.B. Shi, C. Li, Small extracellular vesicle loading systems in cancer therapy: current status and the way forward, Cytotherapy 21 (2019) 1122–1136.

[7] C. He, S. Zheng, Y. Luo, et al., Exosome theranostics: biology and translational medicine, Theranostics 8 (2018) 237–255.

[8] S. Ren, J. Chen, D. Duscher, et al., Microvesicles from human adipose stem cells promote wound healing by optimizing cellular functions via AKT and ERK signaling pathways, Stem Cell Res. Ther. 10 (2019) 47.

[9] A. Liu, D. Lin, H. Zhao, et al., Optimized BMSC-derived osteoinductive exosomes immobilized in hierarchical scaffold via lyophilization for bone repair through Bmpr2/Acvr2b competitive receptor-activated Smad pathway, Biomaterials 272 (2021), 120718.

[10] L. Gao, S. Mei, S. Zhang, et al., Cardio-renal exosomes in myocardial infarction serum regulate proangiogenic paracrine signaling in adipose mesenchymal stem cells, Theranostics 10 (2020) 1060–1073.

[11] G. Lou, Z. Chen, M. Zheng, et al., Mesenchymal stem cell-derived exosomes as a new therapeutic strategy for liver diseases, Exp. Mol. Med. 49 (2017) e346.

[12] S.H.S. Tan, J.R.Y. Wong, S.J.Y. Sim, et al., Mesenchymal stem cell exosomes in bone regenerative strategies - a systematic review of preclinical studies, Mater. Today Bio. 7 (2020), 100067.

[13] X. Wang, P. Thomsen, Basic Clin. Pharmacol. Toxicol. 128 (2021) 18–36.

[14] T. Katsuda, N. Kosaka, F. Takeshita, The therapeutic potential of mesenchymal stem cell-derived extracellular vesicles, Proteomics 13 (2013) 1637–1653.

[15] D.G. Phinney, M.F. Pittenger, Concise review: msc-derived exosomes for cell-free therapy, Stem Cell. 35 (2017) 851–858.

[16] J.O. Jeong, J.W. Han, J.M. Kim, et al., Malignant tumor formation after transplantation of short-term cultured bone marrow mesenchymal stem cells in experimental myocardial infarction and diabetic neuropathy, Circ. Res. 108 (2011) 1340–1347.

[17] O.P. Wiklander, J.Z. Nordin, A. O'Loughlin, et al., Extracellular vesicle in vivo biodistribution is determined by cell source, route of administration and targeting, J. Extracell. Vesicles 4 (2015) 26316.

[18] H.Y. Kim, H. Kumar, M.J. Jo, et al., Therapeutic efficacy-potentiated and diseased organ-targeting nanovesicles derived from mesenchymal stem cells for spinal cord injury treatment, Nano Lett. 18 (2018) 4965–4975.

[19] M.S. Kim, M.J. Haney, Y. Zhao, et al., Engineering macrophage-derived exosomes for targeted paclitaxel delivery to pulmonary metastases: in vitro and in vivo evaluations, Nanomed. UK 14 (2018) 195–204.

[20] J.P. Luyendyk, J.G. Schoenecker, M.J. Flick, The multifaceted role of fibrinogen in tissue injury, Blood 133 (2019) 511–520.

[21] V.L. Stefanelli, T.H. Barker, The evolution of fibrin-specific targeting strategies, J. Mater. Chem. B 3 (2015) 1177–1186.

[22] S. Dmitri, D. Tasmia, H.P. Ji, et al., Biomimetic amplification of nanoparticle homing to tumors, Proc. Natl. Acad. Sci. U. S. A 104 (2007) 932–936.

[23] S. Salunkhe, Dheeraj, M. Basak, et al., Surface functionalization of exosomes for target-specific delivery and in vivo imaging & tracking: strategies and significance, J. Contr. Release 326 (2020) 599–614.

[24] T. Tian, H.X. Zhang, C.P. He, et al., Surface functionalized exosomes as targeted drug delivery vehicles for cerebral ischemia therapy, Biomaterials 150 (2018) 137–149.

[25] H. Yan, X. Mi, A.C. Midgley, et al., Targeted repair of vascular injury by adipose-derived stem cells modified with P-Selectin binding peptide, Adv. Sci. 7 (2020), 1903516.

[26] Q. Zhu, X. Ling, Y. Yang, et al., Embryonic stem cells-derived exosomes endowed with targeting properties as chemotherapeutics delivery vehicles for glioblastoma therapy, Adv. Sci. 6 (2019), 1801899.

[27] C. Théry, S. Amigorena, G. Raposo, et al., Isolation and characterization of exosomes from cell culture supernatants and biological fluids, Curr. Protoc. Cell Biol. 3 (2006), 3.22.21.

[28] D. Eyrich, F. Brandl, B. Appel, et al., Long-term stable fibrin gels for cartilage engineering, Biomaterials 28 (2007) 55–65.

[29] C. Wang, M. Wang, T. Xu, et al., Engineering bioactive self-healing antibacterial exosomes hydrogel for promoting chronic diabetic wound healing and complete skin regeneration, Theranostics 9 (2019) 65–76.

[30] E.B. Petcu, R. Midha, E. McColl, et al., 3D printing strategies for peripheral nerve regeneration, Biofabrication 10 (2018), 032001.

[31] R. Agarwal, A.J. Garcia, Biomaterial strategies for engineering implants for enhanced osseointegration and bone repair, Adv. Drug Deliv. Rev. 94 (2015) 53–62.

[32] J. Zhang, X. Liu, H. Li, et al., Exosomes/tricalcium phosphate combination scaffolds can enhance bone regeneration by activating the PI3K/Akt signaling pathway, Stem Cell Res. Ther. 7 (2016) 136.

[33] S. Yang, S. Guo, S. Tong, et al., Exosomal miR-130a-3p regulates osteogenic differentiation of Human Adipose-Derived stem cells through mediating SIRT7/Wnt/β-catenin axis, Cell Prolif 53 (2020), e12890.

[34] Y. Ji, W. Han, X. Fu, et al., Improved small extracellular vesicle secretion of rat adipose-derived stem cells by microgrooved substrates through upregulation of the ESCRT-III-associated protein Alix, Adv. Healthc. Mater. 10 (2021), 2100492.

[35] M. Wang, C. Wang, M. Chen, et al., Efficient angiogenesis-based diabetic wound healing/skin reconstruction through bioactive antibacterial adhesive ultraviolet shielding nanodressing with exosome release, ACS Nano 13 (2019) 10279–10293.

[36] Y. Zhang, Z. Hao, P. Wang, et al., Exosomes from human umbilical cord mesenchymal stem cells enhance fracture healing through HIF-1α-mediated promotion of angiogenesis in a rat model of stabilized fracture, Cell Prolif 52 (2019), e12570.

[37] W. Ren, J. Hou, C. Yang, et al., Extracellular vesicles secreted by hypoxia pre-challenged mesenchymal stem cells promote non-small cell lung cancer cell growth and mobility as well as macrophage M2 polarization via miR-21-5p delivery, J. Exp. Clin. Cancer Res. 38 (2019) 62.

[38] H. Zhao, Q. Shang, Z. Pan, et al., Exosomes from adipose-derived stem cells attenuate adipose inflammation and obesity through polarizing M2 macrophages and beiging in white adipose tissue, Diabetes 67 (2018) 235–247.

[39] Y. Song, H. Dou, X. Li, et al., Exosomal miR-146a contributes to the enhanced therapeutic efficacy of interleukin-1beta-primed mesenchymal stem cells against sepsis, Stem Cell. 35 (2017) 1208–1221.

[40] P. D. Mosser, M.J. Edwards, Exploring the full spectrum of macrophage activation Nat. Rev. Immunol. 8 (2008) 958–969.

[41] M.E. Ogle, C.E. Segar, S. Sridhar, et al., Monocytes and macrophages in tissue repair: implications for immunoregenerative biomaterial design, Exp. Biol. Med. 241 (2016) 1084–1097.

[42] T. Lopatina, S. Bruno, C. Tetta, et al., Platelet-derived growth factor regulates the secretion of extracellular vesicles by adipose mesenchymal stem cells and enhances their angiogenic potential, Cell Commun. Signal. 12 (2014) 26.

[43] Y. Jia, Y. Zhu, S. Qiu, et al., Exosomes secreted by endothelial progenitor cells accelerate bone regeneration during distraction osteogenesis by stimulating angiogenesis, Stem Cell Res. Ther. 10 (2019) 12.